



A Journal of the Gesellschaft Deutscher Chemiker

Angewandte Chemie

GDCh

International Edition

www.angewandte.org

Accepted Article

Title: Complex Cascade Reaction Networks via Cross β Amyloid Nanotubes

Authors: Chiranjit Mahato, Ayan Chatterjee, and Dibyendu Das

This manuscript has been accepted after peer review and appears as an Accepted Article online prior to editing, proofing, and formal publication of the final Version of Record (VoR). This work is currently citable by using the Digital Object Identifier (DOI) given below. The VoR will be published online in Early View as soon as possible and may be different to this Accepted Article as a result of editing. Readers should obtain the VoR from the journal website shown below when it is published to ensure accuracy of information. The authors are responsible for the content of this Accepted Article.

To be cited as: *Angew. Chem. Int. Ed.* 10.1002/anie.202011454

Link to VoR: <https://doi.org/10.1002/anie.202011454>

COMMUNICATION

Complex Cascade Reaction Networks via Cross β Amyloid Nanotubes

Ayan Chatterjee,[†] Chiranjit Mahato[†] and Dibyendu Das^{*[a]}

Abstract: Biocatalytic reaction networks integrate complex cascade transformations via spatial localization of multiple enzymes confined within the cellular milieu. Inspired by Nature's ingenuity, we demonstrate that short peptide based cross- β amyloid nanotubular hybrids can promote different kinds of cascade reactions, from simple two-step, multistep to complex convergent cascades. The compartmentalizing ability of paracrystalline cross- β phases was utilized to colocalize sarcosine oxidase (SOX) and hemin as artificial peroxidase. Further, the catalytic potential of the amyloid nanotubes with ordered arrays of imidazoles were used as hydrolase mimic. The designed SOX-hemin amyloid nano hybrids featuring a single extant enzyme could integrate different logic networks to access complex digital designs with the help of three concatenated AND gates and biologically relevant stimuli as inputs.

Multistep network reactions in biological systems were shaped through millions of years of evolution.^[1] In extant biological processes, cascades involving divergent, convergent, coupled, or sequential steps lead to diverse chemical transformations that are complex yet synchronized.^[2] These cascades play critical roles in the living systems, from cellular metabolism, signal transduction to feedback guided oscillatory reactions on regulatory functions and so forth.^[2a,3] Compartmentalized environments featuring spatially confined multiple enzyme complexes within subcellular organelles act as microreactors for simultaneous oxidative and biosynthetic pathways to build essential biomolecules and catabolize energy sources. The team play between enzymes, where products of one biocatalyst act as substrates for others, enrich the local reactant concentrations which lead to improved proficiency of the complex cascade transformations.^[3b,4-7] Mimicking such systems can have implications in the design of enzymatic fuel cells, disease diagnostics, biosensors, catalysis and synthesis of pharmaceuticals.^[8] Further, defining such complex chemical networks can contribute to our understanding of the emerging field of systems chemistry.^[9]

Towards this end, we argued that the paracrystalline surfaces of short amyloid phases could behave as self-assembled organelles that can foster complex cascade reactions. Cross β amyloid phases accessed by short peptides are known for their remarkable binding capabilities towards diverse guests, from small molecules to large macromolecules.^[10-12] Further, the inherent catalytic abilities of the repetitive amyloid structures are often argued as the earliest protein folds.^[13-15] Herein, we have utilized the binding and catalytic potential of the cross- β amyloid to load sarcosine oxidase (SOX) and a prosthetic group hemin to devise nano hybrids that promote two-step, three-step, and

convergent cascades (Figure 1). Further, we demonstrate the generation of complex bio-computed logic systems that used multiple inputs and three-concatenated AND gates.

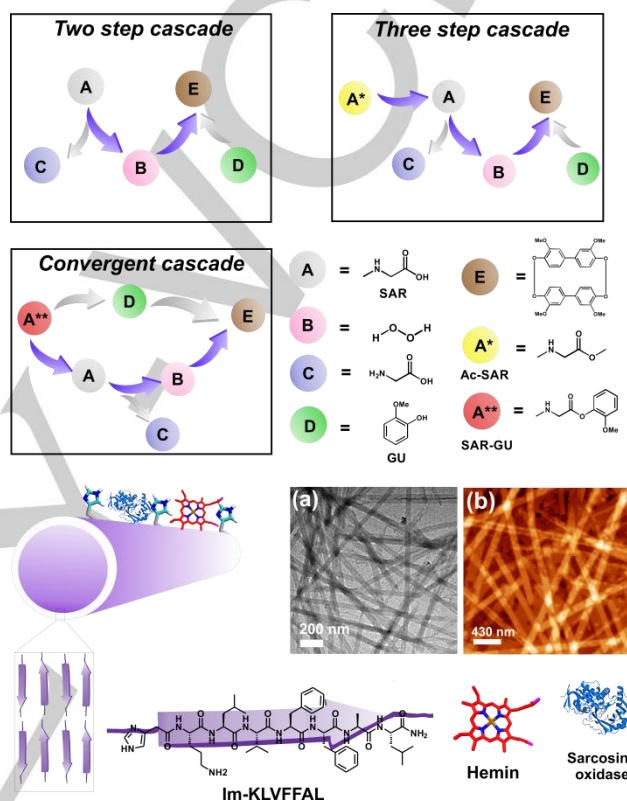


Figure 1. Schematic representation of different types of cascade reactions on the surface of amyloid nanotube. TEM (a) and AFM (b) of the Im-KLVFFAL (Im-KL) nanotubes, respectively.

We used the hydrophobic nucleating core (¹⁷LVFFA²¹) of wild type A β (1-42) sequence recognized for protein deposits seen in Alzheimer's disease.^[8c,11-12] The pentapeptide has been shown to access diverse morphologies with the propensity to non-covalently bind proteins as well as small molecules.^[11c-e] The termini modification of this core leads to Im-KLVFFAL-NH₂ (Im-KL, Figure 1) which assembles into homogeneous nanotubes (diameter=50 \pm 10 nm, height=7.6 \pm 0.7 nm, Figure 1, S1). Characteristic β -sheet signature with the antiparallel arrangement was observed from CD and FTIR respectively (Figure S2-3).^[14,15a,b] Powder X-ray diffraction (PXRD) showed reflection at d-spacing of 4.67 Å and 10.63 Å which corresponded to the H-bonded β -strand and β -sheet laminate distances respectively (Figure S4).^[14a] To probe the surface exposure of imidazoles and lysines, negatively charged gold nanoparticles (GNPs) were added. Ordered arrays of GNPs on the nanotube surface were

[a] Department of Chemical Sciences & Centre for Advanced Functional Materials, Indian Institute of Science Education and Research (IISER) Kolkata, Mohanpur, West Bengal, 741246, India E-mail: dasd@iiserkol.ac.in

[†] A.C. and C.M. contributed equally.

COMMUNICATION

observed, suggesting the presence of solvent-exposed cationic groups that help in colloidal stability (Figure S5).^[14a]

To exploit Im-KL nanotubes for templating a simple two-step oxidase-peroxidase cascade, SOX, a peroxisomal enzyme in mammals and sarcosine-inducible enzyme in soil bacteria, was used.^[16a] The flavoenzyme catalyzes oxidative demethylation of sarcosine (SAR) to glycine, formaldehyde and simultaneous formation of H_2O_2 , which fuels the second reaction (Figure 2).^[16a-c] Rather than using an additional enzyme, we explored the possibility of hemin bound amyloid folds to act as a peroxidase.^[11e] Hemin, present in extant peroxidases and metalloenzymes, has low intrinsic peroxidase activity in the free state.^[11e] Hemin bound nanotubes were characterized thoroughly using UV Vis spectroscopy. Free hemin (pH 8 buffer) showed Soret peak at 388 nm and a broad shoulder peak at 366 nm indicating the presence of dimeric (μ -oxo bihemin) and some monomeric hemin hydroxide (haematin). A low-intensity Q band at around 620 nm also suggested the presence of μ -oxo bihemin in free state.^[17] In contrast, hemin bound to nanotubes showed Soret peak at 412 nm and charge transfer transitions at ca. 626 and 530 nm, suggesting imidazole-hemin coordination (Figure S6).^[17] Notably, the peak intensity of bound hemin at 366 nm was very weak in comparison to free state. This suggested reduction of dimerization and formation of monomeric haematin on nanotube surface.^[17d]

To calculate loading, Im-KL nanotube was exposed to different amounts of hemin, incubated for 30 min followed by ammonium hydroxide washes to remove non-specifically bound hemin (SI).^[18a] Loading was calculated to be $79.8 \pm 5 \mu\text{g}\cdot\text{mg}^{-1}$ with the help of standard plot (Figure S7-8). Notably, at lower concentrations (up to $5 \mu\text{M}$), all hemin was found to be loaded on the surface. To generate Im-KL-hemin-SOX nanohybrid, hemin ($5 \mu\text{M}$) loaded nanotube was exposed to SOX ($5 \mu\text{M}$). From Bradford Assay, entire enzyme concentration was observed to be bound to the nanotubes (SI). AFM showed distinct globular structures on the nanotube surface with line analysis demonstrating increase of height from ca. $7.6 \pm 0.7 \text{ nm}$ to $11.1 \pm 1.8 \text{ nm}$ (Figure 2b). We further used CLSM to analyze the co-localization of hemin and SOX on the nanotube surface through fluorescein labelled hemin and rhodamine B isothiocyanate (RITC) tagged SOX.^[18b] At excitation of $\lambda=490 \text{ nm}$, CLSM showed fluorescent fibrillar networks (Figure 2c). Notably, when excited at 556 nm , distinct nanotubular networks were clearly visualized that corresponded to the RITC labeled SOX (Figure 2c). Notably, the software-merged image indicated the overlapping of fluorescent fibrillar morphologies, thus underpinning the co-localization of the two guests.

For the two-step cascade reaction, the activity was monitored by adding the substrate SAR along with guaiacol (GU) as the well-known chromogenic substrate.^[16d] We expected that the bound SOX will aerobically oxidize SAR to generate H_2O_2 which will be subsequently utilized by hemin to catalyze the oxidation of GU to a brown product (Figure 2a). The kinetics of tetraguaiacol product formation was monitored by UV-Vis spectroscopy ($\lambda_{\text{max}}=470 \text{ nm}$, Figure 2d,e). The activity of the cascade by Im-KL-hemin-SOX was found to be $6.4 \pm 0.8 \mu\text{M}\cdot\text{min}^{-1}$ with 25 mM of SAR (Figure 2e, S9). Interestingly, cascade activity in the presence of nanotubes was 8.5-fold higher compared to the controls of free hemin-SOX-histidine diffusional mixture at the same concentration. When

separately used, SOX bound Im-KL and hemin bound Im-KL, they did not show any noticeable activity (Figure 2e, S9). This result suggested that the co-localization of the catalysts on the amyloid surface helped in facilitating the cascade reaction via increasing the local concentration of the substrates.

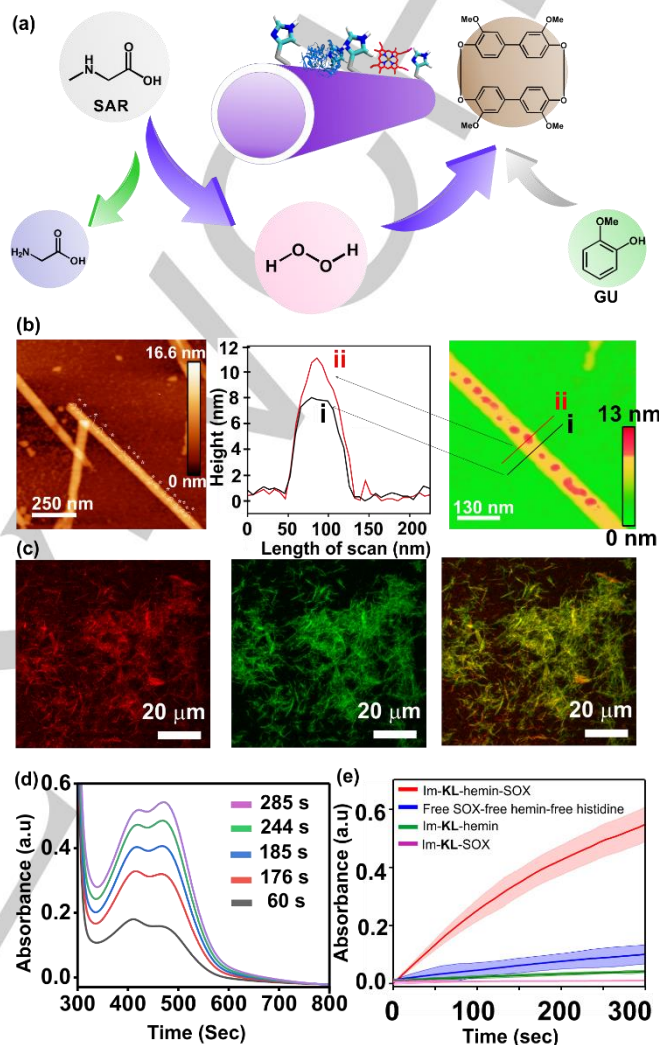


Figure 2. (a) Schematic representation of two-step cascade reaction. (b) AFM images of SOX bound to Im-KL (left), line scans (center) and colour-coded AFM images for heights (right). (c) CLSM images of Im-KL bound to RITC-labelled SOX (left), FITC-labelled hemin (center), and merged image (right). (d) UV absorbance spectra ($\lambda_{\text{max}}=470 \text{ nm}$) and (e) kinetic spectra of the two-step cascade reaction monitored at $\lambda_{\text{max}}=470 \text{ nm}$.

At this point, we sought to explore the intrinsic hydrolase-like activity of the imidazole exposed amyloid surfaces that could facilitate the three-step biocatalytic cascade reaction.^[14] For this purpose, we used acetylated sarcosine (Ac-SAR) which can be hydrolyzed to SAR by the imidazole exposed amyloid nanotubes (Figure 3a). Subsequently, in the second step, SOX bound to nanotubes will consume SAR to generate H_2O_2 which would act as substrate for GU oxidation catalyzed by bound hemin (Figure 3a). Interestingly, the three-step cascade product was indeed formed when Ac-SAR was added to Im-KL-hemin-SOX (2.03 ± 0.6

COMMUNICATION

$\mu\text{M}\cdot\text{min}^{-1}$, Figure 3b, S10). To the best of our knowledge, this is the first example of a three-step cascade reaction where only one comparatively smaller enzyme is used instead of three large enzymes. The activity of Im-KL-hemin-SOX was 26-fold higher compared to the free diffusional mixture of SOX, hemin and histidine at equal concentrations ($0.08\pm 0.04 \mu\text{M}\cdot\text{min}^{-1}$, Figure 3b, S10). To probe the hydrolytic role of imidazole moiety, we replaced it with an acetyl group (Ac-KLVFFAL, Ac-KL). Ac-KL assembled to form indistinguishable nanotubular structures as seen for Im-KL (diameter $32\pm 3 \text{ nm}$, Figure S11).^[12b,15b] Notably, activity for Ac-KL decreased significantly ($0.14\pm 0.1 \mu\text{M}\cdot\text{min}^{-1}$, Figure 3c, S12) and thus highlighted the vital role of imidazoles of Im-KL. Further, we added free histidine to Ac-KL which indeed augmented the activity ($0.55\pm 0.8 \mu\text{M}\cdot\text{min}^{-1}$) but still was 3.6-fold lower compared to Im-KL (Figure 3c, S12). These results corroborated the crucial role of the arrays of imidazoles installed on the Im-KL surface for the hydrolysis step of the multistep cascade reaction.

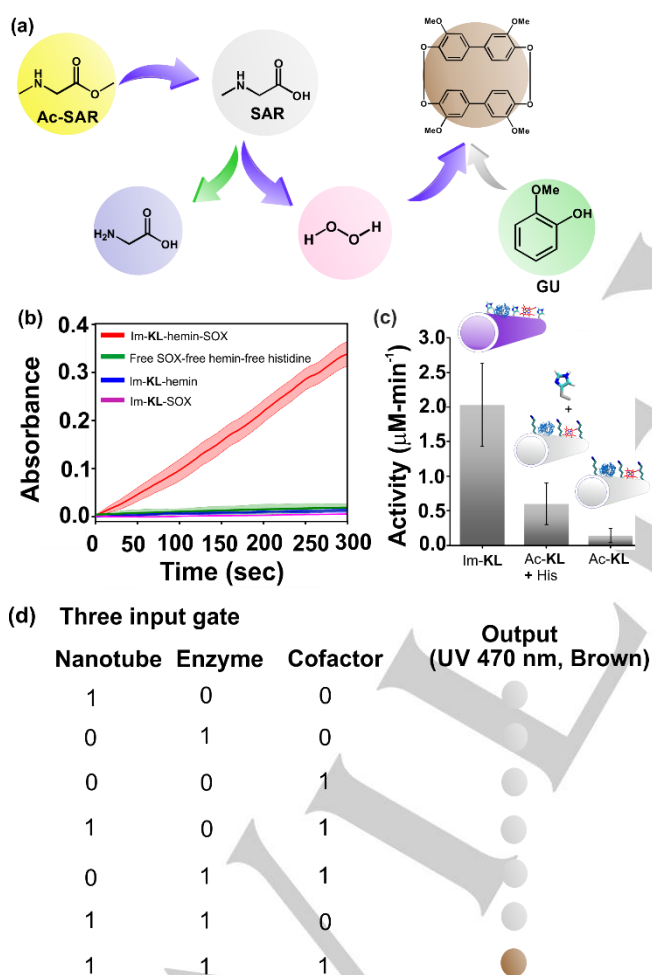


Figure 3. Schematic representation of three-step cascade, b) Time-dependent kinetics of the three-step cascade reaction, c) bar diagram of the cascade

activity by SOX-hemin bound Im-KL, Ac-KL and Ac-KL with histidine, d) Three-input Boolean AND logic gate, by SOX, hemin, and Im-KL as the chemical inputs.

The use of molecule-based logic gates has emerged as an exciting tool for many potential applications.^[19] Biological processes take place in the aqueous milieu and are connected by various electrochemical and supramolecular interactions. Hence, logic gates in wet platform utilizing inputs such as metabolites, pH, ions and so for the while providing useful outputs (colour, fluorescence etc.) can be useful in processing the chemical/biochemical information.^[19] To highlight the significance of every component of the nanohybrid for the multistep cascade, AND gate was constructed with peptide, SOX, and hemin as the inputs and absorbance at 470 nm as output which could also be seen with the naked eye (Figure 3d). When any one of the components of Im-KL-hemin-SOX was used as the input (1,0,0/0,1,0/0,0,1), the reaction did not cascade to the output (0). The combination of two components (1,1,0/1,0,1/0,1,1) also resulted in no output (0). Only the incorporation of all three inputs (1,1,1) resulted in the output (1, Figure 3d).

We sought to construct a complex convergent cascade system which is seen in protein signaling and nervous systems.^[2] We coupled two critical inputs of the cascade, SAR and GU to form an ester (SAR-GU) with the expectation that Im-KL nanotubes will hydrolytically release the components (Figure 4a). SAR-GU will thus provide SAR, which will be degraded to H_2O_2 that will subsequently converge with the other fragment (GU). Remarkably, the cascade product was indeed formed by Im-KL-hemin-SOX as confirmed from the colour change of the medium within 30 s of the reaction. Figure 4b shows the time course generation of the product (red curve) whereas controls show very low rates. The cascade activities of Im-KL-hemin-SOX ($13.4\pm 2 \mu\text{M}\cdot\text{min}^{-1}$) were 30-fold higher than those of free SOX, hemin and histidine mixtures ($0.44\pm 0.2 \mu\text{M}\cdot\text{min}^{-1}$, Figure S13). This significant improvement of activity could be attributed to the substrate channelling effect where the generated H_2O_2 was rapidly consumed by the proximally located hemin in presence of in-situ generated GU. As control, freshly disassembled Im-KL in presence of unbound hemin and SOX was used (Figure S14, S1). The activity was found to be very low ($0.8\pm 0.3 \mu\text{M}\cdot\text{min}^{-1}$) which underpinned the importance of co-localization of hemin and SOX on the surface of the nanotube. Kinetic study further suggested that the hydrolysis step was slower compared to the terminal oxidation step (Figure S15-17). Moreover, to understand this aspect, we divided Im-KL-hemin-SOX into two parts. Half of the nanotubes were incubated with SOX and the other half with hemin in separate microcentrifuge tubes so that each batch of nanotubes will feature only one particular guest. The activity of this mixture was found to be 45% of the native activity (Figure S18). We argued that the complexity of a chemically system is not only limited to a single Boolean logic operation (AND or OR) but can

COMMUNICATION

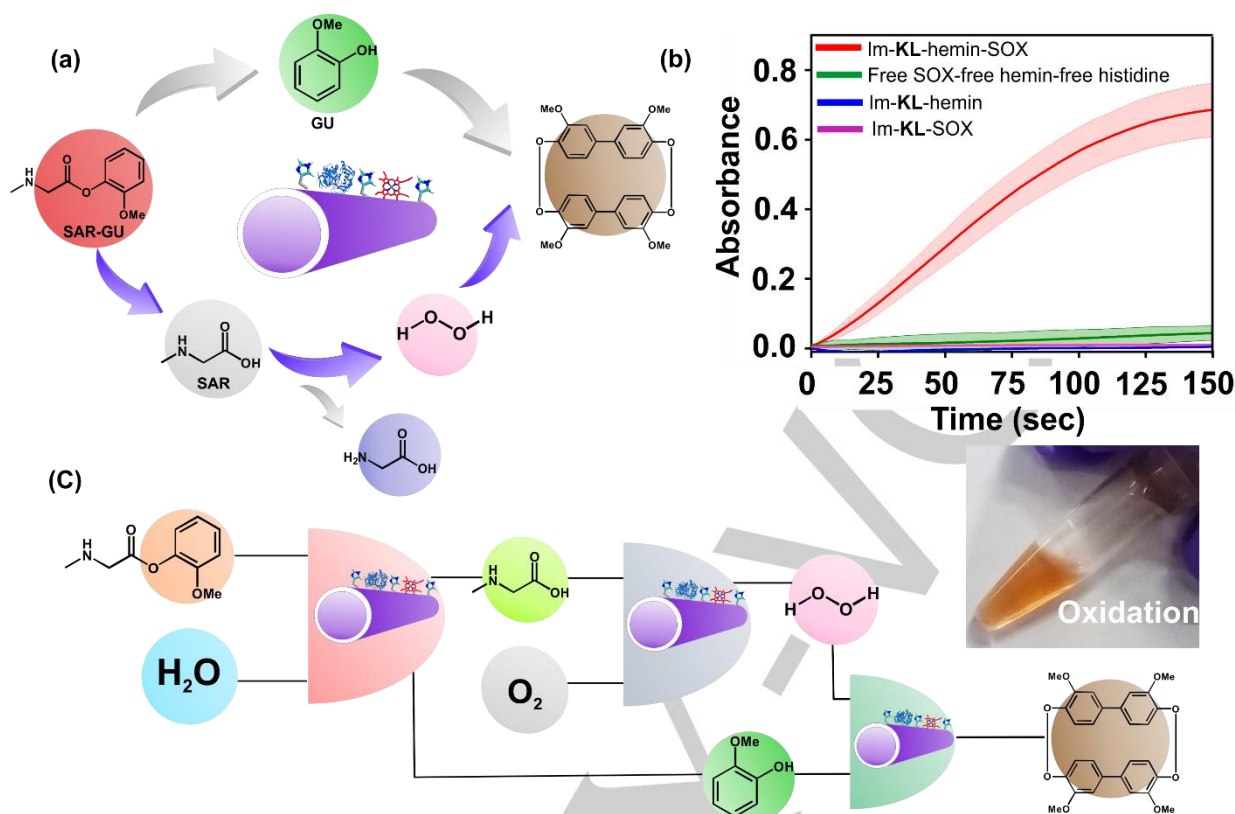


Figure 4. a) Schematic representation of convergent cascade, b) Time-dependent kinetics of different systems, c) Logic network representation of the cascade reaction with different Chemical Input Signals and inset showing the image of the chromogenic output.

be extended to the construction of complex combinatorial multi-gate logic networks. This usually required compatible inputs that can cascade the information throughout the networks to provide the output. A three-concatenated AND gate was constructed utilizing multiple biologically important stimuli as inputs (Figure 4c). The operation made by Im-KL-hemin-SOX on the inputs i.e. SAR-GU and H₂O, resulted in the output of SAR and GU, thus successfully constructing an AND gate. Subsequently, one more AND gate was constructed with the help of inputs oxygen (dissolved in water), SAR (output of first AND gate). Interestingly, output of the first AND gate i.e. GU and the output of second AND gate i.e. H₂O₂ converged as the inputs for a third AND gate resulting in the final output (color) via concatenation of AND gates (Figure 4c). Unprecedentedly, three sequential AND gates were integrated within a simple chemical system where output and input from different steps converge to make a closed network. Such complexity is seen in convergent signalling pathways of extant biology.

In summary, the present study demonstrates the generation of a single enzyme based nanohybrid that can facilitate diverse cascade reactions, from two-step, multistep to complex convergent cascades. The nanotubular hybrids were created by loading enzyme SOX and molecular hemin on the paracrystalline imidazole rich surface of short peptide based amyloid assemblies. Further, complex digital design of combinatorial chemoelectronic logic networks has been proposed with the help of suitable

chemical inputs that foreshadowed the convergent cascade. The general strategy and design flexibility of such amyloid nanohybrids make the developed systems adaptable for accessing intelligent soft material.

Experimental Section

Experimental details in supporting information.

Acknowledgements

For financial support, DD, AC and CM are thankful to SERB (EMR/2017/005126), DST, GOI., CSIR and Nano Mission (SR/NM/NS-1082/2015) respectively.

Keywords: Amyloid • Peptide Self-assembly • Enzyme Mimics • complex cascade • Logic gates

1. a) J. A. Bradford, K. A. Dill, *Proc. Natl. Acad. Sci. USA* **2007**, *104*, 10098–10103; b) C. R. Woese, *Proc. Natl. Acad. Sci. USA*, **2002**, *99*, 8742–8747.
2. a) N. Ramos-DeSimone, E. Hahn-Dantona, J. Siple, H. Nagase, D. L. French, J. P. Quigley, *J. Biol. Chem.* **1999**, *274*, 13066–13076; b) D. Bray, *Nature* **1995**, *376*, 307–313.

COMMUNICATION

3. a) G. M. Cooper, *The Cell: A Molecular Approach* (Sinauer Associates, Sunderland, **2000**); b) N. A. Thornberry, Y. Lazebnik, *Science* **1998**, *281*, 1312–1316.
4. a) I. Wheeldon, S. D. Minter, S. Banta, S. C. Barton, P. Atanassov, M. Sigman, *Nat. Chem.* **2016**, *8*, 299–309; b) K. S. Rabe, J. Muller, M. Skoupi, C. M. Niemeyer, *Angew. Chem. Int. Ed.* **2017**, *56*, 13574–13589; *Angew. Chem.* **2017**, *129*, 13574–13589; c) S. N. Semenov, A. S. Wong, R. M. van der Made, S. G. Postma, J. Groen, H. W. van Roekel, T. F. de Greef, W. T. Huck, *Nat. Chem.* **2015**, *7*, 160–165.
5. a) Y. Zhang, S. Tsitkov, H. Hess, *Nat. Catal.* **2018**, *1*, 276–281; b) X. Zhao, H. Palacci, V. Yadav, M. M. Spiering, M. K. Gilson, P. J. Butler, H. Hess, S. J. Benkovic, A. Sen, *Nat. Chem.* **2018**, *10*, 311–317.
6. a) O. I. Wilner, Y. Weizmann, R. Gill, O. Lioubashevski, R. Freeman, I. Willner, *Nat. Nanotechnol.* **2009**, *4*, 249–254; b) W. H. Chen, M. Vázquez-González, A. Zoabi, R. Abu-Reziq, I. Willner, *Nat. Catal.* **2018**, *1*, 689–695; c) C. W. Chiang, X. Liu, J. Sun, J. Guo, L. Tao, W. Gao, *Nano Lett.* **2020**, *20*, 1383–1387; d) J. Liang, F. Mazur, C. Tang, X. Ning, R. Chandrawati, K. Liang, *Chem. Sci.* **2019**, *10*, 7852–7858; e) S. Dutta, N. Kumari, S. Dubbu, S. W. Jang, A. Kumar, H. Ohtsu, J. Kim, S. H. Cho, M. Kawano, I. S. Lee, *Angew. Chem. Int. Ed.* **2020**, *59*, 3416–3422; *Angew. Chem.* **2020**, *132*, 3444–3450.
7. a) R. S. Rikken, H. Engelkamp, R. J. Nolte, J. C. Maan, J. C. van Hest, D. A. Wilson, P. C. Christianen, *Nat. Commun.* **2016**, *7*, 12606; b) Y. Men, W. Li, Y. Tu, F. Peng, G. A. Janssen, R. J. M. Nolte, D. A. Wilson, *ACS Nano* **2019**, *13*, 12767–12773; c) X. Zhao, H. Palacci, V. Yadav, M. M. Spiering, M. K. Gilson, P. J. Butler, H. Hess, S. J. Benkovic, A. Sen, *Nat. Chem.* **2018**, *10*, 311–317; d) A. Somasundar, S. Ghosh, F. Mohajerani, L. N. Massenburg, T. Yang, P. S. Cremer, D. Velegol, A. Sen, *Nat. Nanotechnol.* **2019**, *14*, 1129–1134; e) B. Saha, A. Chatterjee, A. Reja, D. Das, *Chem. Commun.* **2019**, *55*, 14194–14197.
8. a) Z. Zhu, T. Kin Tam, F. Sun, C. You, Y. H. Percival Zhang, *Nat. Commun.* **2014**, *5*, 3026; b) Y. Zhang, M. A. Arugula, M. Wales, J. Wild, A. L. Simonian, *Biosens. Bioelectron.* **2015**, *67*, 287–295; c) T. O. Omosun, M. C. Hsieh, W. S. Childers, D. Das, A. K. Mehta, N. R. Anthony, T. Pan, M. A. Grover, K. M. Berland, D. G. Lynn, *Nat. Chem.* **2017**, *9*, 805–809; d) P. Makam, S. Yamijala, K. Tao, L. Shimon, D. Eisenberg, M. Sawaya, B. Wong, E. Gazit, *Nat. Catal.* **2019**, *2*, 977–985.
9. a) D. Kroiss, G. Ashkenasy, A. B. Braunschweig, T. Tuttle, R. V. Uljin, *Chem* **2019**, *5*, 1917–1920; b) M. Frenkel-Pinter, M. Samanta, G. Ashkenasy, L. J. Leman, *Chem. Rev.* **2020**, *120*, 4707–4765; c) M. Bagnani, G. Nyström, C. D. Michele, R. Mezzenga, *ACS Nano* **2019**, *13*, 591–600.
10. a) Sanz, S. de Marcos, J. Galban, *Biosens. Bioelectron.* **2007**, *22*, 2876–2883; b) K. Tao, B. Xue, Q. Li, W. Hu, L. J. W. Shimon, P. Makam, M. Si, X. Yan, M. Zhang, Y. Cao, R. Yang, J. Li, E. Gazit, *Mater. Today (Kidlington)* **2019**, *30*, 10–16; c) S. Ahmed, A. Chatterjee, K. Das, D. Das, *Chem. Sci.* **2019**, *10*, 7574–7578; d) R. Freeman, M. Han, Z. Álvarez, J. A. Lewis, J. R. Wester, N. Stephanopoulos, M. T. McClellon, C. Lynsky, J. M. Godbe, H. Sangji, E. Luijten, S. I. Stupp, *Science* **2018**, *362*, 808–813.
11. a) G. Wei, Z. Su, N. P. Reynolds, P. Arosio, I. W. Hamley, E. Gazit, R. Mezzenga, *Chem. Soc. Rev.* **2017**, *46*, 4661–4708; b) W. S. Childers, A. K. Mehta, K. Lu, D. G. Lynn, *J. Am. Chem. Soc.* **2009**, *131*, 10165–10172; c) N. Kapil, A. Singh, D. Das, *Angew. Chem. Int. Ed.* **2015**, *54*, 6492–6495; *Angew. Chem.* **2015**, *127*, 6592–6595; d) A. Reja, S. P. Afrose, D. Das, *Angew. Chem. Int. Ed.* **2020**, *59*, 4329–34; *Angew. Chem.* **2020**, *132*, 4359–4364; e) A. Chatterjee, S. P. Afrose, S. Ahmed, A. Venugopal, D. Das, *Chem. Commun.* **2020**, *56*, 7869–7872.
12. a) T. P. Knowles, R. Mezzenga, *Adv. Mater* **2016**, *28*, 6546–6561; b) N. Kapil, A. Singh, M. Singh, D. Das, *Angew. Chem. Int. Ed.* **2016**, *55*, 7772–7776; *Angew. Chem.* **2016**, *128*, 7903–7907; c) J. Greenwald, M. P. Friedmann, R. Riek, *Angew. Chem. Int. Ed.* **2016**, *55*, 11609–11613; *Angew. Chem.* **2016**, *128*, 11781–11785; d) J. Greenwald, R. Riek, *J. Mol. Biol.* **2012**, *421*, 417–426; e) M. Reches, E. Gazit, *Science* **2003**, *300*, 625–627.
13. a) J. Greenwald, W. Kwiatkowski, R. Riek, *J. Mol. Biol.* **2018**, *430*, 3735–3750; b) R. Bomba, S. K. Rout, M. Bütikofer, W. Kwiatkowski, R. Riek, J. Greenwald, *Orig. Life Evol. Biosph.* **2019**, *49*, 213–224; c) A. K. Mehta, K. Lu, W. S. Childers, Y. Liang, S. N. Dublin, J. Dong, J. P. Snyder, S. V. Pingali, P. Thiagarajan, D. G. Lynn, *J. Am. Chem. Soc.* **2008**, *130*, 9829–9835.
14. a) B. Sarkhel, A. Chatterjee, D. Das, *J. Am. Chem. Soc.* **2020**, *142*, 4098–4103; b) C. Zhang, R. Shafi, A. Lampel, D. MacPherson, C. Pappas, V. Narang, T. Wang, C. Madarelli, R. V. Uljin, *Angew. Chem. Int. Ed.* **2017**, *56*, 14511–14515; *Angew. Chem. Int. Ed.* **2017**, *129*, 14703–14707; c) P. W. Frederix, G. G. Scott, Y. M. Abul-Haija, D. Kalafatovic, C. G. Pappas, N. Javid, N. T. Hunt, R. V. Uljin, T. Tuttle, *Nat. Chem.* **2015**, *7*, 30–37; d) C. M. Rufo, Y. S. Moroz, O. V. Moroz, J. Stohr, T. A. Smith, X. Hu, W. F. DeGrado, I. V. Korendovych, *Nat. Chem.* **2014**, *6*, 303–309; e) M. O. Guler, S. I. Stupp, *J. Am. Chem. Soc.* **2007**, *129*, 12082–12083; f) S. Onogi, H. Shigemitsu, T. Yoshii, T. Tanida, M. Ikeda, R. Kubota, I. Hamachi, *Nat. Chem.* **2016**, *8*, 743–752; g) J. Ottelé, A. S. Hussain, C. Mayer, S. Otto, *Nat. Catal.* **2020**, *3*, 547–553; h) J. R. Fores, M. C. Gonzalez, A. Chaumont, A. Carvalho, C. Blanck, M. Schmutz, F. Boulmedais, P. Schaaf, L. Jiery, *Angew. Chem. Int. Ed.* **2020**, *59*, 14558–14563; *Angew. Chem. Int. Ed.* **2020**, *132*, 14666–14671; i) I. Insua, J. Montenegro, *J. Am. Chem. Soc.* **2020**, *142*, 300–307; j) C. Z.-J. Ren, P. S. Muñana, G. G. Warr, J. L.-Y. Chen, *ACS Catal.* **2020**, *10*, 8395–8401.
15. a) M. R. Elkins, T. Wang, M. Nick, H. Jo, T. Lemmin, S. B. Prusiner, W. F. DeGrado, J. Stohr, M. Hong, *J. Am. Chem. Soc.* **2016**, *138*, 9840–9852; b) S. Li, A. N. Sidorov, A. K. Mehta, A. J. Bisignano, D. Das, W. S. Childers, E. Schuler, Z. Jiang, T. M. Orlando, K. Berland, D. G. Lynn, *Biochemistry* **2014**, *53*, 4225–4227.
16. a) A. Goyer, T. L. Johnson, L. J. Olsen, E. Collakova, Y. Shachar-Hill, D. Rhodes, A. D. Hanson, *J. Biol. Chem.* **2004**, *279*, 16947–53; b) H. Suzuki, *Amino Acids* **1994**, *7*, 27–43; c) M. A. Wagner, M. S. Jorns, *Biochemistry* **2000**, *39*, 8825–8829; d) J. J. Ridge, *Br. Med. J.* **1903**, *1*, 1257.
17. a) Y. Gao, F. Zhao, Q. Wang, Y. Zhang, B. Xu, *Chem. Soc. Rev.* **2010**, *39*, 3425–3433; b) J. Babul, E. Stellwagen, *Biochemistry* **1972**, *11*, 1195–1200; c) T. Yonetani, H. Anni, *J. Biol. Chem.* **1987**, *262*, 9547–9554; d) Q. Wang, Z. Yang, X. Zhang, X. Xiao, C. K. Chang, B. Xu, *Angew. Chem. Int. Ed.* **2007**, *46*, 4285–4289; *Angew. Chem.* **2007**, *119*, 4363–4367; e) Q. Liu, H. Wang, X. Shi, Z. G. Wang, B. Ding, *ACS Nano* **2017**, *11*, 7251–7258; f) Wang, Z. Yang, L. Wang, M. Ma, B. Xu, *Chem. Commun.* **2007**, *0*, 1032–1034.
18. a) I. Nakamichi, A. Habtezion, B. Zhong, C. H. Contag, E. C. Butcher, M. B. Omary, *J. Clin. Invest.* **2005**, *115*, 3007–3014; b) Y. Zhang, F. Lyu, G. Jun, Z. Liu, *Chem. Commun.* **2014**, *50*, 12919–12922.
19. a) S. Erbas-Cakmak, S. Kolemen, A. C. Sedgwick, T. Gunnlaugsson, T. D. James, J. Yoon, E. U. Akkaya, *Chem. Soc. Rev.* **2018**, *47*, 2228–2248; b) P. Zhang, D. Gao, K. An, Q. Shen, C. Wang, Y. Zhang, X. Pan, X. Chen, Y. Lyv, C. Cui, T. Liang, X. Duan, J. Liu, T. Yang, X. Hu, J. J. Zhu, F. Xu, W. Tan, *Nat. Chem.* **2020**, *12*, 381–390; c) A. Eordogh, C. Paganini, D. Pinotsi, P. Arosio, P. Rivera-Fuentes, *ACS Chem. Biol.* **2020**, doi.org/10.1021/acchembio.0c00639; d) X. Dai, K. Han, Z. Ma, H. Han, *Adv. Funct. Mater.* **2018**, *28*, 1804609; e) Z. Chen, R. D. Kibler, A. Hunt, F. Busch, J. Pearl, M. Jia, Z. L. VanAernum, B. I. M. Wicky, G. Dods, H. Liao, M. S. Wilken, C. Ciarlo, S. Green, H. El-Samad, J. Stamatoyannopoulos, V. H. Wysocki, M. C. Jewett, S. E. Boyken, D. Baker, *Science* **2020**, *368*, 78–84; f) M. Ikeda, T. Tanida, T. Yoshii, K. Kurotani, S. Onogi, K. Urayama, I. Hamachi, *Nat. Chem.* **2014**, *6*, 511–518.

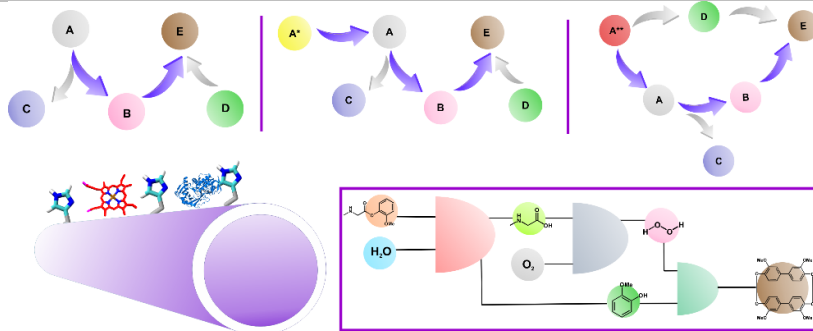
COMMUNICATION

Entry for the Table of Contents (Please choose one layout)

Layout 1:

COMMUNICATION

Complex Cascade-effect: Amyloid based minimalistic systems have been shown to demonstrate diverse cascade reaction networks, starting from simple two-step, multistep to complex convergent cascades. Further, complex chemoelectronic computations were done with the help of multi input, concatenated AND gates.



Ayan Chatterjee,[†]
Chiranjit Mahato[†]
and Dibyendu Das^{*}

Page No. – Page No.

Complex Cascade
Reaction
Networks via
Cross β Amyloid
Nanotubes